Simulation of Wave Forces on a Gravity Based Foundation by a BEM Based on Fully Nonlinear Potential Flow

Jeffrey C. Harris[1], *Konstantin Kuznetsov*[1], *Christophe Peyrard*[1,2], *Sylvain Saviot*[2], *Amin Mivehchi*[3], *Stephan T. Grilli*[3], *Michel Benoit*[4]

(1) LHSV, Ecole des Ponts, CEREMA, EDF R&D, Université Paris-Est, Chatou, France
(2) EDF R&D, Laboratoire National d'Hydraulique et Environnement, Chatou, France
(3) Dept. of Ocean Engineering, University of Rhode Island, Narragansett, RI 02882, USA
(4) Institut de Recherche sur les Phénomènes Hors Equilibre (IRPHE),
UMR 7342 (Aix-Marseille Univ., Ecole Centrale Marseille, CNRS), Marseille, France

ABSTRACT

We report on recent developments of a three-dimensional (3D) model for wave propagation and wave-structure interaction. The velocity field is solved with a boundary element method (BEM), based on fully non-linear potential flow. This approach is efficiently parallelized on CPU clusters. Recent progress is presented for extending the model for the use of higher-order elements (i.e., cubic B-splines), and outline the future steps necessary to a high-order approach on completely arbitrary meshes necessary for complex industrial applications. Particular care is taken with regards to the corner compatibility condition along the intersection between the body and free-surface, which is necessary for high-accuracy modeling with the BEM approach. Applications are shown for academic tests as well as for the computation of wave-induced forces and moments on gravity-based foundations, where we compare numerical results against laboratory experiments. Such applications are of interest to the continued development of foundations for offshore wind farms, and extensions to this model are being implemented for simulating floating structures and coupling to other models including viscous effects, which can be important in some cases.

INTRODUCTION

A large variety of ocean wave models have been applied to investigate wave-structure interaction; ever since the work of Longuet-Higgins and Cokelet (1976), the boundary integral approach based on potential flow theory has shown some interesting advantages, particularly as the calculations are only performed on the surfaces and not the interior of the domain. In the models, different ways to handle the free-surface have been proposed, both in frequency and time-domain, but in some cases where fully nonlinear effects are important, the standard approach has been to solve Laplace's equation for the velocity potential (mass conservation) at each time step (optionally multiple times, or for the time-derivative of the velocity potential), then updating the BEM mesh nodes and free surface boundary conditions with a mixed Eulerian-Lagrangian (MEL) approach. Tanizawa (2000) made a review to date of this technique.

Here, we use such a fully nonlinear potential flow (FNPF) model, based on a boundary element method (BEM), similar to the approach of Grilli et al. (2001). Their model has been successful at accurately modeling landslide-generated tsunamis, rogue waves, waves generated by a surface effect ship, and the initiation of wave breaking caused by bathymetry. The higher-order BEM implemented by Grilli et al. was based on a type of elements called "cubic mid-interval interpolation" (MII), which worked on a structured grid (Fig. 2); this approach worked well in the absence of surface-piercing structures. More recent work, however, has focused on using more flexible unstructured grids that could handle surface-piercing fixed or floating bodies, but using linear elements (Harris et al., 2014a); this was less accurate, but the grid could more easily represent an arbitrary geometry. Additionally, the model efficiency was improved by using the Fast Multipole Method (FMM Greengard and Rokhlin (1987)) implemented on parallel CPU clusters for larger grids (Harris et al., 2014b). This FMM-BEM approach has been validated for wave propagation as well as radiation and diffraction around vertical cylinders (Dombre, 2015).

Nonlinear wave-structure interaction is particularly important for offshore structures because of the phenomenon of ringing, that can cause high peak loads. Molin (2002) provides a summary of this problem. For industrial applications, nonlinear forces can be estimated to some degree by using Volterra transfer functions, as discussed by Kim (2008).

In this paper, we return to questions of accuracy of the BEM solution by implementing cubic B-spline boundary elements, which enables higher-accuracy results on the same mesh as previously used with linear elements, and even in some cases yield a better performance than MII elements. There is no space here for a complete literature review on the subject, but Maestre et al. (2016) has created one example of a recently developed spline-based Numerical Wave Tank (NWT). Here we endeavor to achieve something similar, showing improvements over earlier versions of our model built on similar methods.

METHODOLOGY

For an incompressible inviscid fluid with irrotational motion, mass conservation is a Laplace's equation for the velocity potential, ϕ,

$$\nabla^2 \phi = 0 \qquad \text{in D} \tag{1}$$

$$\mathbf{u} = \nabla \phi \qquad \text{in D} \tag{2}$$

with $\mathbf{u}$ the flow velocity in domain D (e.g., Fig. 1). Using a semi-Lagrangian approach on the free-surface, for which points are fixed in the horizontal direction, the material derivative for a point following the

free-surface reads:

$$\frac{\delta}{\delta t} = \frac{\partial}{\partial t} + \frac{\partial \eta}{\partial t} \frac{\partial}{\partial z} \tag{3}$$

where η denotes the vertical position of the free surface. From this, we can express the kinematic and dynamic free surface boundary conditions in Cartesian coordinates, in a reference frame that is potentially moving in the x-direction at a speed, $U(t)$, as:

$$\frac{\delta \eta}{\delta t} = \frac{\partial \phi}{\partial z} - \frac{\partial \phi}{\partial x} \frac{\partial \eta}{\partial x} - \frac{\partial \phi}{\partial y} \frac{\partial \eta}{\partial y} - U(t) \frac{\partial \eta}{\partial x} \tag{4}$$

$$\frac{\delta \phi}{\delta t} = -g\eta - \frac{1}{2}\nabla\phi \cdot \nabla\phi + \frac{\partial \eta}{\partial t} \frac{\partial \phi}{\partial z} - U(t) \frac{\partial \phi}{\partial z} \tag{5}$$

with g the gravitational acceleration, z the vertical coordinate, p the fluid pressure (assumed to be zero on the free surface), and ρ the fluid density.

On stationary submerged or surface-piercing bodies, the boundary condition is simply a no-flow condition on the body boundary (or hull) Γ_h, whereas for bodies moving relative to the coordinate system, with fixed or free motion, which are not considered in this paper, the boundary condition expresses that the normal flow velocity matches that of the rigid body projected on the local normal direction. Numerically damping waves exiting at the edge of the domain in direction x is handled by adding $-\nu(x)\eta$ and $-\nu(x)\phi$ to the right side of Eq. 4 and 5, respectively, where $\nu = 0$ for all of the domain except for points $x \geq x_{AB}$, where $\nu(x) = \nu_0 \left(\frac{x - x_{AB}}{L_{AB}} \right)^2$.

Hydrodynamic forces and moments acting on the rigid body are computed by integrating the hydrodynamic pressure. This requires calculating the time derivative of the potential at each time step, which also satisfies Laplace's equation; here, as in Grilli et al.'s NWT (Grilli et al., 2001), $\partial\phi/\partial t$ is also computed with a BEM. For freely moving bodies, however, both BEMs for the potential and its time derivative are coupled through the unknown body motion, which requires implementing special procedures (see, e.g., Guerber et al. (2012) for a review and details).

Boundary element method

As indicated above, Laplace's Eq. 1 is solved as a BIE expressed at each collocation point $\mathbf{x}_i$ (or $[x_i, y_i, z_i]$ for $i = 1, \ldots, N$),

$$\alpha(\mathbf{x}_i)\phi(\mathbf{x}_i) = \int \left[\frac{\partial \phi}{\partial n}(\mathbf{x})G(\mathbf{x}, \mathbf{x}_i) - \phi(\mathbf{x})\frac{\partial G}{\partial n}(\mathbf{x}, \mathbf{x}_i) \right] d\Gamma \tag{6}$$
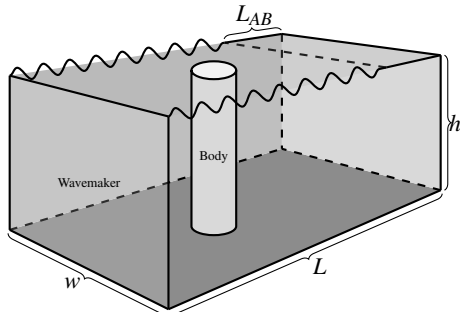

Fig. 1: Definition sketch of NWT computational domain for wave interaction with a rigid body (length L by width w by depth h). No-flow conditions are specified on lateral and bottom boundaries; waves are generated on the leftward boundary (Neumann boundary condition for known velocity and acceleration) and are damped on the far end of the NWT over an absorbing beach (AB) of length L_{AB}.

where G is the free space Green's function based on the distance to the target point i, $\mathbf{r}_i = \|\mathbf{x}_i - \mathbf{x}\|$, α is the exterior solid angle made by the boundary at a collocation point i (e.g., for a smooth boundary this would be 2π), and $\mathbf{n}$ points in the direction of the local outwards normal vector to the boundary. In 3D, the free space Green's function of Laplace's equation and its normal derivative read:

$$G(\mathbf{x}, \mathbf{x}_i) = \frac{1}{4\pi\|\mathbf{r}_i\|} \tag{7}$$

$$\frac{\partial G}{\partial n}(\mathbf{x}, \mathbf{x}_i) = -\frac{1}{4\pi}\frac{\mathbf{r}_i \cdot \mathbf{n}}{\|\mathbf{r}_i\|^3} \tag{8}$$

Solving Eq. 6 with a BEM discretization requires: (i) integrating integral kernels over individual boundary elements, which become singular when $\mathbf{r}_i \to 0$; and (ii) solving the resulting (typically N by N) linear system of algebraic equations. The BEM integrals are performed over each triangular element using Dunavant (1984) rules, and quadrangular elements with a tensor product of Gauss integration. Singular integrals are dealt with using a Duffy transformation (Duffy, 1982). The coefficients α in the BIE are found by applying the rigid mode method (e.g., Grilli et al. (1989)), which expresses that for a Dirichlet problem with $\phi = 1$ specified over the entire boundary of domain D, the discretized BIE must yield $\partial\phi/\partial n = 0$; the α coefficients are then found as the residuals of this Dirichlet problem. The solution of the BEM discretized algebraic system is then solved with GMRES, a Krylov iterative solver.

Parallelization

On modern computers, it is often advantageous to run the model over a distributed cluster, sharing the workload over different processors. This is relatively simple to do with a BEM: when applying Eq. 6, each processor uses an approximately equal partition of the number of elements, thus each processor stores a piece of the resulting system matrix.

This savings in time also applies to the GMRES solver, where each matrix-vector product is also parallelized, and combined on a single node. This corresponds to expressing the algebraic system as $Ax = (A_1 + A_2 + \ldots + A_n)x$ where each A_i corresponds to the contribution to the system matrix from each processor. The matrix assembly and matrix-vector products required, which take the most amount of computational time, are thus efficiently divided.

Significant work has been done in using the fast multipole method (FMM) with this same code, including some described in a corresponding paper at this conference (Mivehchi et al. 2017), but here we do not focus on this. Use of the FMM permits the CPU time of the resulting code for large problems to be as fast as $O(N)$ instead of $O(N^2)$ when using GMRES with a standard BEM (Greengard and Rokhlin, 1987).

The NWT detailed here is thus not ideal, but nevertheless relatively efficient, and unaffected by changes to the time-stepping and element types, which are discussed next.

Time-stepping

For fluid-structure interaction it is advantageous (and for freely-moving structures, often necessary for reasons of stability) to solve the problem not only for the velocity potential but also for its time-derivative, in determining the pressure on a body. Having $\partial\phi/\partial t$ available, as in Grilli et al. (2001), we could perform the time updating of both the free surface and body position in the NWT based on second-order Taylor series, which more efficiently makes use of the information available.
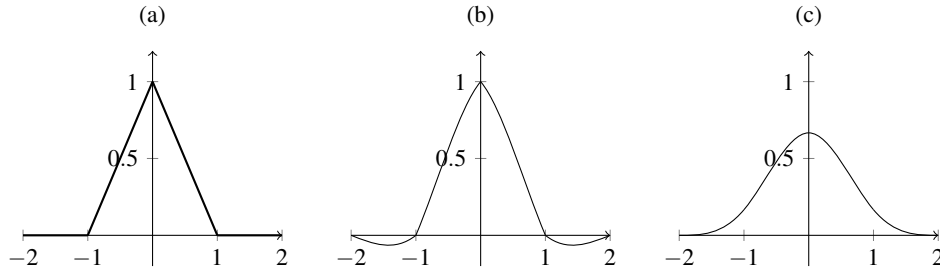
Fig. 2: Equivalent one-dimensional (1D) basis function for the BEM elements considered in this paper: (a) linear; (b) MII; (c) cubic B-spline.

Here we instead use a third-order Runge-Kutta explicit scheme for time updating, which can be written compactly as:

$$f^{(1)} = f^{(n)} + \Delta t (\delta_t f^{(n)}) \tag{9}$$

$$f^{(2)} = \frac{3}{4} f^{(n)} + \frac{1}{4} \left(f^{(1)} + \Delta t (\delta_t f^{(1)}) \right) \tag{10}$$

$$f^{(n+1)} = \frac{1}{3} f^{(n)} + \frac{2}{3} \left(f^{(2)} + \Delta t (\delta_t f^{(2)}) \right) \tag{11}$$

As a result of this, we can make a direct comparison with any type of element, as long as we can compute the normal vector at each point of the moving boundaries, as well as the velocity from the known values of ϕ and ϕ_n at a given time step.

In particular, to solve Eq. (4), we note that for a normal vector $\mathbf{n} = (n_x, n_y, n_z)$:

$$\frac{\partial \eta}{\partial x} = \frac{-n_x}{n_z} \quad \text{and} \quad \frac{\partial \eta}{\partial y} = \frac{-n_y}{n_z} \tag{12}$$

The flow velocity can also be derived in the same coordinate system (Fochesato et al., 2005). If we define a coordinate system based on unit-vectors ($\mathbf{s}, \mathbf{m}, \mathbf{n}$) where $\mathbf{s}$ and $\mathbf{m}$ are tangent to the surface, we note that these vectors may be non-orthogonal, and we define $\kappa = \mathbf{s} \cdot \mathbf{m} \in [0, 1]$. Further, we obtain the normal vector from: $\mathbf{n} = \mathbf{s} \times \mathbf{m}$. This yields the velocity:

$$\mathbf{u} = (\phi_s - \kappa\phi_m)/(1 - \kappa^2)\mathbf{s} + (\phi_m - \kappa\phi_s)/(1 - \kappa^2)\mathbf{m} + \phi_n\mathbf{n} \tag{13}$$

In the case of linear elements, where the derivatives may not be continuous at a given point, we take the velocity at a collocation node to be an average of the velocity on the adjacent elements.

Cubic B-splines

Considering a BEM model, the geometry problem is defined uniquely by the boundary surfaces of the fluid domain, so accurate description of boundary surfaces is important for the accuracy of the entire model. We consider here cubic B-splines, which are widely used by the computer aided design (CAD) systems to accurately describe complex surfaces.

The use of cubic B-splines is for all field variables, which includes coordinates, velocity potential, and its normal derivative. The goal of cubic B-spline interpolation is to obtain a smooth surface with continuous first and second derivatives, both on the surface of each element and at each collocation node.

If we consider a one-dimensional (1D) version, a tabulated function $g_k = g(s_k), k = 0, ..., N$ is a list of values at different points. The cubic B-spline function, $S(s)$ in $[s_0, s_N]$ could be written as the linear combination of the B_k:

$$S(s) = \sum_{k=-1}^{N+1} p_k B_k(s), \tag{14}$$

where p_k is a unknown value at control points, B_k are the basis functions that satisfy C_2 continuity conditions (from which the second deivative is continuous), and $S(s_k) = g_k$ at control points s_k. Unknown values p_k can then be calculated by solving a system of linear equations:

$$g_k = \frac{1}{6} p_{k-1} + \frac{4}{6} p_k + \frac{1}{6} p_{k+1}. \tag{15}$$

for all k, because $B(-1) = 1/6$, $B(0) = 4/6$, and $B(+1) = 1/6$. This step is different than using linear or MII elements, for example, because in those other cases the basis functions in 1D would be one at the center and zero at all other integer valued points (see Fig. 2).

To use this B-spline algorithm and solving for control points in 2D, we can use the tensor product B-spline interpolation and express an interpolated function $S(s, m)$ as:

$$S(s, m) = \sum_{i=-1}^{N+1} \sum_{j=-1}^{M+1} p_{ij} B_i(s) B_j(m), \tag{16}$$

Similar to the algorithm for 1D B-splines we can then construct a matrix of coefficients for every control point. The tensor products of B-spline are shown at Fig. 3. We only need to construct this linear system once at teach time step, which we can later solve and use to interpolate different physical parameters over the mesh.

At the edges of each B-spline surface, we need to add additional equations in the system; for edges we consider so-called not-a-knot conditions, described below. We apply these boundary conditions by adding a single layer of virtual nodes along each edge (Fig. 3).

Not-a-knot condition The not-a-knot condition assumes that the third-derivative of the B-spline is continuous between the two intervals at the edge of the surface. In 1D, we can represent this by:

$$p_{k-1} - 4p_k + 6p_{k+1} - 4p_{k+2} + p_{k+3} = 0. \tag{17}$$

Equivalent coefficients for 2D B-splines are shown in Fig.3e. This condition is used because we do not generally know, for example, both the value and the derivative of the parameters at the edges of a surface. However, improvements could be made later for the velocity potential, ϕ, making use of physical information from the intersecting surfaces to specify derivative, as in Grilli and Svendsen (1990).
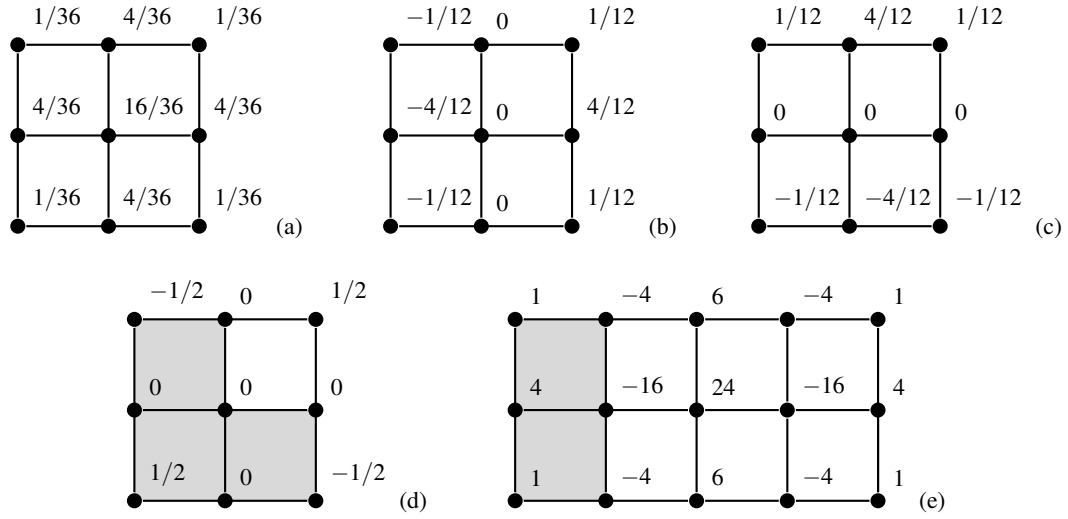
Fig. 3: Coefficients needed for computing 2D B-splines: (a) control points; (b) partial derivative in *s*-direction; (c) partial derivative in *m*-direction. In lower panel, examples are shown for coefficients used in: (d) cross derivative in *sm* directions for corner condition; (e) not-a-knot condition. Grayed out sections are so-called "virtual" elements beyond the edge of a surface.
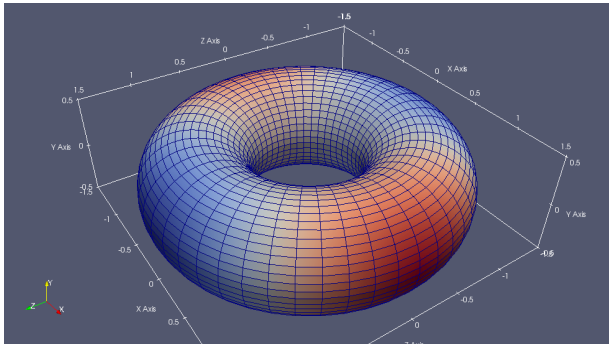

Fig. 4: Torus-shaped domain for testing the accuracy of B-splines versus linear BEM elements.

Fig. 5: Errors corresponding to the velocity computed on a torus with the test function $\phi = x^2 - z^2$, with different element types.

Corner condition For simplicity, we implement the assumption that $\partial_{sm} = 0$ in the corners. Coefficients for that case shown are in Fig.3d.

In the future we will use a more arbitrary grid connectivity, perhaps T-splines (Sederberg et al., 2003), to describe surfaces instead of B-splines. T-splines are a generalization of B-splines, in which several B-spline patches can be integrated into unique T-spline, so that it is possible to describe surfaces and boundary parameters more accurately.

PERFORMANCE TESTING

Velocity errors for different element types

In order to test the implementation of B-splines, we first start with a test case that does not involve edges or corners. In this case, to create a regular grid, the natural choice would be a torus. We choose one whose major radius of 1.0 and minor radius 0.5 (Fig. 4).

After creating such a mesh, we can determine the normal vector at each collocation point, and then apply a test function, $\phi^{(test)} = x^2 - z^2$, with the corresponding normal derivative, $\phi_n^{(test)} = 2xn_x - 2zn_z$. After that
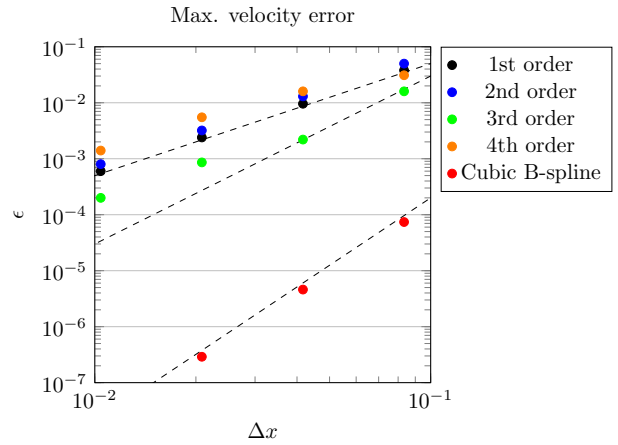
we can compute the velocity at each point. We then consider the error associated with such result:

$$\varepsilon = \frac{\max(||\mathbf{u} - \mathbf{u}^{(test)}||)}{\max(||\mathbf{u}^{(test)}||)} \tag{18}$$

Fig. 5 shows this errors as a function of grid size.

In all cases, the error decreases with a refining mesh, indicating convergence to the proper solution. We also see that higher-order isoparametric elements produce more accurate results, but only up to a certain point: if we increase the order of the polynomial interpolation too much, the error no longer decreases as fast, because of larger errors at the edge of each element; this is related to Runge's phenomenon for polynomial interpolation. By contrast, we see that B-splines provide much more accurate results for the same order element on the same mesh.

There are different methods for dealing with the loss of accuracy of higher-order isoparametric elements, including spectral elements (i.e.,
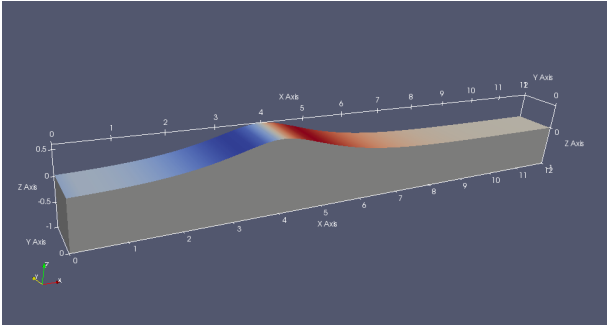
Fig. 6: Propagation in the NWT of a solitary wave of height $H/h_0 = 0.6$ in a grid of non-dimensional dimensions 12x1x1 for testing the accuracy and convergence of the BEM solution as a function of grid size N (or equivalent mesh size Δx) and element type.

adjusting the positions of the collocation nodes) or a mid-interval interpolation (the MII element of Grilli et al. (2001)), etc.

Solitary wave propagation

A standard test case for nonlinear wave models is the propagation of solitary waves, and checking for errors in volume and energy. Similar to Grilli and Svendsen (1990) in 1D and Grilli et al. (2001) in 2D, we first assess the convergence properties of the NWT in terms of conservation of mass and energy, as a function of a non-dimensional grid resolution $\beta = \sqrt{\Delta x/g}/\Delta t$, reflecting mesh and time step size, for the propagation over a constant depth h_0 of a solitary wave of large height H (Fig. 6).

Note, in their error analysis, Grilli et al. used instead the mesh Courant number, $C_o = (\Delta t \sqrt{gh_0})/\Delta x$. Here we use β as introduced by Büchmann (2000) who proposed that the accuracy and stability of results of such NWTs is better described as a function of a mesh Froude number, since the most unstable modes correspond to the shortest wavelengths. [In fact, the mesh Courant number used by Grilli et al. (2001) is easily related to β, as $C_0 = \beta^{-1}\sqrt{h_0/\Delta x}$, so there is a one-to-one correspondence between the two approaches.] Comparing errors on mass and energy against β, we see in Fig. 7 distinct trends in the results.

In the simulations, the NWT has a length 12 times the water depth, a width equal to depth, and the wave is such that $H/h_0 = 0.6$. As in Grilli et al. (2001), the solitary wave profile and its initial potential and normal velocity on the free-surface are computed using the method of Tanaka (1986), and the crest is initially located at $x' = x/h_0 = 4$; computations are performed until $t' = t\sqrt{g/h_0} = 3.2$ (prime variables are non-dimensional, with length being scaled by depth h_0 and time by $\sqrt{h_0/g}$). We compare results obtained here for the mass and energy errors parameters with those reported by Grilli et al. (2001) using their 3D-NWT with cubic MII elements; in the present simulations results are either obtained with cubic B-spline elements or with linear elements. In the MII and B-spline cases, we use the same structured grid of $N = 1,030$ nodes, corresponding to a grid spacing on the free surface of $\Delta x = 0.25h_0$, and adjust the time step. With linear elements, we use an unstructured triangular mesh of $N = 1,242$ nodes and approximately the same grid spacing, in order to compare all the results with each other.

At each time step, we compute the numerical error on the global conservation of mass and total energy of the solitary wave. During propagation, both mass and energy of the solitary wave should theoretically stay constant, as there is no mass or energy input or output into the NWT. Hence, we define the numerical error on wave volume as: $\varepsilon_m = |(m(t) - m_0)/m_0|$, with the instantaneous solitary wave volume being computed in the NWT as:

$$m(t) = \int_{\Gamma_f} z n_z \, d\Gamma \tag{19}$$

with Γ_f denoting the free surface boundary, and m_0 the theoretical value obtained with Tanaka's method. Similarly, we define the numerical error on total wave energy as $\varepsilon_e = |(e(t) - e_0)/e_0|$, with the instantaneous total energy being computed as the sum of kinetic and potential energy, as:

$$e(t) = \frac{1}{2}\rho \int_{\Gamma} \phi \frac{\partial \phi}{\partial n} \, d\Gamma + \frac{1}{2}\rho g \int_{\Gamma_f} z^2 n_z \, d\Gamma \tag{20}$$

and e_0 being again the theoretical value obtained with Tanaka's method. In both equations, some integrals are taken only over the free surface, which allows computing the part of the volume and potential energy error corresponding to the wave only, which is a stricter condition than computing relative errors with respect to the entire NWT mass and energy and thus avoids underestimating errors for large NWTs in which much of the water is not in motion.

One sees that accuracy in terms of mass or volume conservation is substantially better with cubic B-splines than any other. It appears to be less
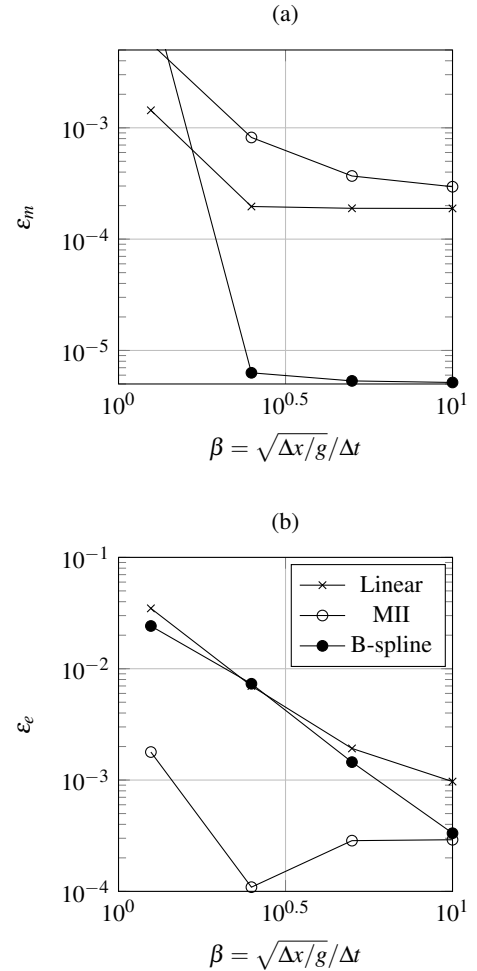

Fig. 7: Maximum errors in volume (top) and energy (bottom) conservation for propagating a solitary wave with amplitude of $H/h = 0.6$, for MII (hollow), linear (x), and B-spline (solid) NWTs.
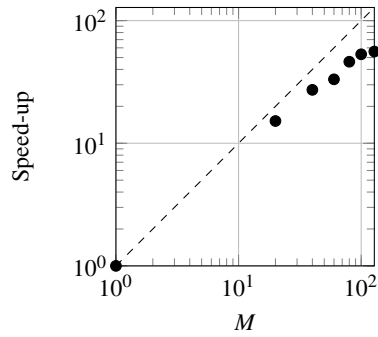
Fig. 8: Parallel scaling of the BEM solution of Laplace's equation for a mesh of quadrangular cubic B-spline elements with $N = 1,030$ nodes, as a function of the number M of CPU cores; 36 integration points were used over each element.

accurate with MII elements, but since the grid stretches as it follows the wave, as opposed to a semi-Lagrangian (fixed horizontal position), this may be the cause. In contrast, energy conservation is best with the MII code, and the difference between unstructured triangular mesh and cubic B-splines is not very significant, suggesting that for this size mesh, the error is determined mostly by the time-stepping method. Future work will investigate whether it is possible to improve this accuracy further.

We can also assess the efficiency of the parallelization on this application. Fig. 8 shows that up to several hundred processors, the scaling is relatively efficient. Thus while for a single processor the B-spline code is slower than the highly optimized MII code, as the earlier code of Grilli et al. (2001) is not parallel, for a large enough computer we are able to match the same "wall-clock", or simulation time in terms of the real world. Certainly for larger meshes we also need to look at implementing the FMM with cubic B-spline elements, which has already been done for linear elements in Harris et al. (2016).

GRAVITY BASED FOUNDATION

Experimental setup

As a part of earlier (1/45 scale) model testing by France Energies Marines, a study was made of a gravity based foundation (GBF) that could be used, e.g., to support offshore wind turbines (Fig. 9). This would correspond at full scale to a diameter at the waterline of 6.5 m, and the diameter at the bottom of the conical part of 20 m; the foundation itself is 30 m across. The conical part starts 2 m above the mudline and ends 12 m above the it. Experimental results were acquired for regular and irregular sea states, as well as both with and without current. Here we consider only the smallest wave states, in order to avoid numerical instabilities which can exist along waterlines.

The tests were performed in a 80-m long and 1.5-m wide wave flume in which waves were generated with a wavemaker, which were both regular (Table 1) or irregular (not discussed here) waves. Nonlinear wave modeling is performed with the NWT, which is believed to be important due to the experimental results, which show that in some instances, ringing was observed. Of particular interest is the surge force or overturning moment (Fig. 10).
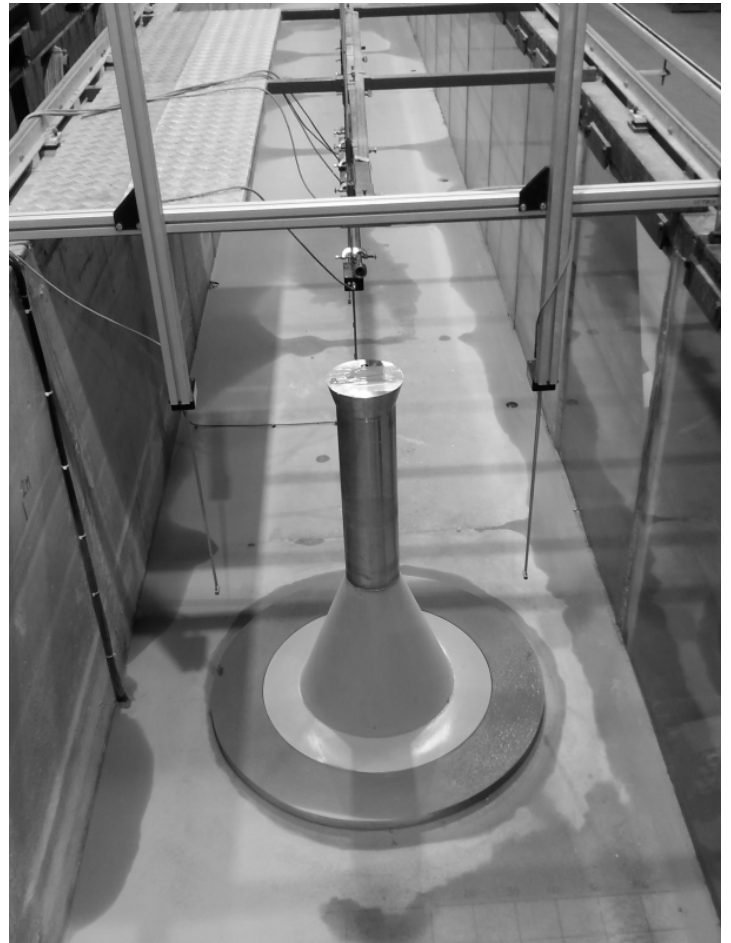

Fig. 9: Gravity based foundation model at 1/45 scale in empty wave flume.

Test	Wave height	Wave period	Depth	Current
02-R	5.6 m	8.6 s	30.0 m	0.0 m/s
04-R	9.3 m	9.8 s	30.0 m	0.0 m/s
05-R	13.0 m	10.3 s	30.0 m	0.0 m/s
02-RC	5.6 m	8.6 s	30.0 m	+1.0 m/s
04-RC	9.3 m	9.8 s	30.0 m	+1.0 m/s
05-RC	13.0 m	10.3 s	30.0 m	+1.0 m/s
02-RCM	5.6 m	8.6 s	30.0 m	-1.0 m/s
04-RCM	9.3 m	9.8 s	30.0 m	-1.0 m/s
05-RCM	13.0 m	10.3 s	30.0 m	-1.0 m/s
U1-R	13.7 m	10.9 s	34.1 m	0.0 m/s
U1-RC1	13.7 m	10.9 s	34.1 m	+1.0 m/s

Table 1: Regular wave tests on gravity based foundation, showing target wave conditions at prototype scale.

Fig. 12: Typical instability seen near the free-surface for modeling the O2-R or larger waves.
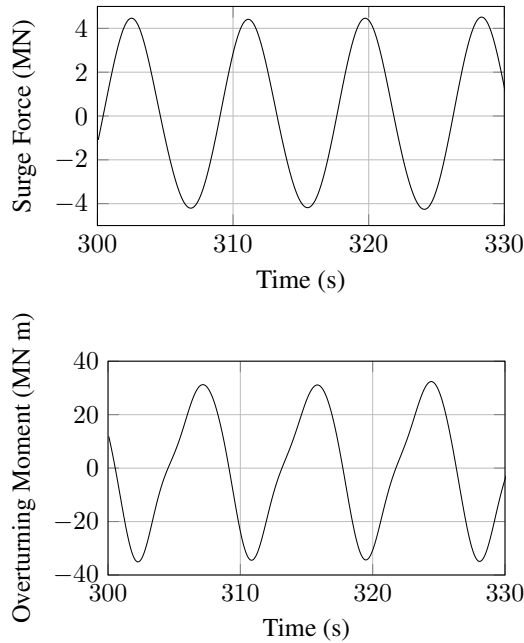
Fig. 10: Time series of surge force (top panel) and overturning moment on the GBF structure (lower panel) of Fig. 9, for case O2-R.

Numerical comparisons

Here we consider the O2-R test case (Table 1), with a wave height of 5.6 m and a wave period of 8.6 s. At present, although large amplitude waves appear to be modeled well (e.g., the solitary wave above), and tests with earlier versions of the model for interactions with monopiles show reasonable results for higher-order harmonics (e.g., comparisons by Harris et al. (2016) with data of Huseby and Grue (2000)) with steepnesses up to $kA = 0.15$. Cases here, however, are at least at $kA = 0.16$ for the O2-R case, and some substantially higher. In these cases, instabilities along the waterline become an issue (Fig. 12).

It has been reported that nonlinear NWT models can be unstable near waterlines, and a variety of approaches have been proposed for handling this, generally based on filtering short, presumably nonphysical, wavelengths (Tanizawa, 2000); others have considered more complex timestepping schemes (e.g. Mola et al., 2013) to deal with this. (A substantial filtering naturally stabilizes the problem but may affect the physics.)

As a result, we can make an estimate of the NWT with cubic B-spline
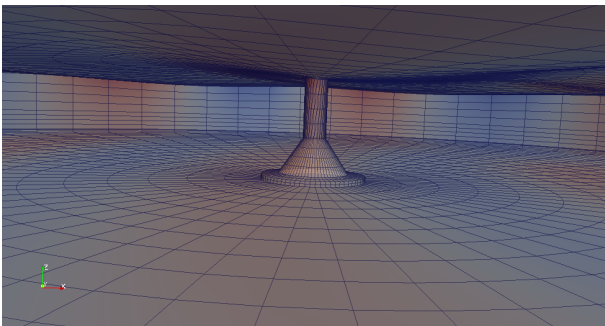

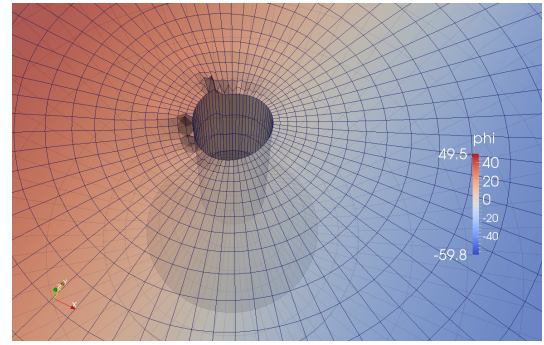Fig. 11: Numerical GBF numerical grid, with cubic B-splines.

elements (i.e., using a grid of Fig. 11, with a timestep of 0.1 s), but with a reduced, 2 m wave height. Then, we can consider the Fourier transform of the force (or equivalently, the moment) as:

$$f^{(m)}(t) = \int_t^{t+T} \left(\int_{body} p \, dA \right) e^{im\omega\tau} d\tau \qquad (21)$$

From this, assuming that the nondimensional coefficients, $f^{(n)}/(\rho g A^n)$ are constant for different wave amplitudes, we were able to estimate the value by reconstructing the time-series based on the coefficients with the smaller amplitude (e.g., for the third harmonic of the overturning moment, $M_y^{(3)}(H = 5.6m) \approx (5.6/2.0)^3 M_y^{(3)}(H = 2m)$). This is essentially the approach of Volterra transfer functions, as discussed by Kim (2008), and data for monopiles (e.g. Huseby and Grue, 2000) shows that this can be a reasonable approximation for moderate wave amplitudes. Clearly this is approximate, but shows potential should the instability be resolved.

From this, we obtain a range of overturning moment from -44 to +34 MN m and a surge force between -5.0 and +4.9 MN (Fig. 13), which corresponds well to the experimental results (Fig. 10). The model in its present form takes approximately an hour and a half with 256 processors, running in parallel. More complex tests, with larger incident wave heights, will be shown at the conference, testing different ways to stabilize these short waves near the waterline (see e.g. Guignard and Grilli, 2001; Grilli et al., 2003), which may be damped in the basin tests due to viscous effects.

SUMMARY

In this paper, we demonstrated a numerical wave tank (NWT) for solving fully nonlinear potential flows using the boundary element method (BEM). This NWT uses a higher-order spatial discretization with cubic B-splines, enabling more accurate results than using other element types. In addition, the model is parallelized to work on hundreds of CPUs.

Comparisons with earlier versions of the code show large gains in accuracy relative to linear elements, and even compared to cubic mid-interval interpolation of Grilli et al. (2001), at least for some limited test cases. We further presented results in particular for a GBF, which could be used as the foundation of an offshore wind turbine, showing reasonable agreement with experimental results for an initial test.

A variety of changes are required to complete this as an industrial tool, namely: integration of the cubic B-spline representation into the fast multiple method algorithm (FMM; see Mivehchi et al. in this conference for
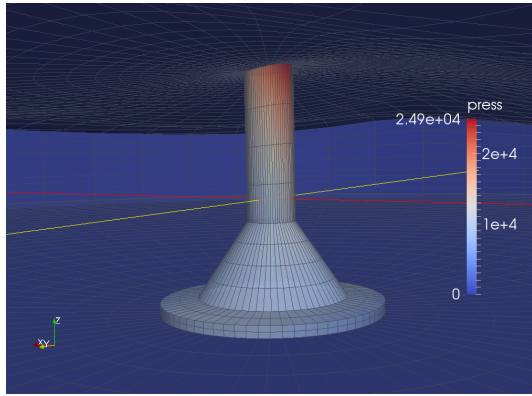
Fig. 13: Hydrodynamic pressure on the GBF at an instant.

some details on this point); switching to Taylor series time-stepping as in Grilli et al. (2001); handling of arbitrary grid connectivity. Progress towards these goals will be presented at the conference.

ACKNOWLEDGEMENTS

REFERENCES

Büchmann, B. (2000). "Accuracy and stability of a set of free-surface time-domain boundary element models based on B-splines". *International Journal for Numerical Methods in Fluids*, 33:125–155.

Dombre, E. (2015). *Modélisation non-linéaire des interactions vague-structure appliquée à des flotteurs déoliennes off-shore*. PhD thesis, Université Paris-Est.

Duffy, M. G. (1982). "Quadrature over a pyramid or cube of integrands with a singularity at a vertex". *SIAM Journal on Numerical Analysis*, 19:1260–1262.

Dunavant, D. A. (1984). "High degree efficient symmetrical Gaussian quadrature rules for the triangle". *International Journal for Numerical Methods in Engineering*, 21:1129–1148.

Fochesato, C., Grilli, S. T., and Guyenne, P. (2005). "Note on non-orthogonality of local curvilinear co-ordinates in a three-dimensional boundary element method". *International Journal for Numerical Methods in Fluids*, 48:305–324.

Greengard, L. and Rokhlin, V. (1987). "A fast algorithm for particle simulations". *Journal of Computational Physics*, 73:325–348.

Grilli, S. T., Guyenne, P., and Dias, F. (2001). "A fully nonlinear model for three-dimensional overturning waves over arbitrary bottom". *International Journal for Numerical Methods in Fluids*, 35:829–867.

Grilli, S. T., Skourup, J., and Svendsen, I. A. (1989). "An efficient boundary element method for nonlinear water waves". *Engineering Analysis with Boundary Elements*, 6:97–107.

Grilli, S. T. and Svendsen, I. A. (1990). "Corner problems and global accuracy in the boundary element solution of nonlinear wave flows". *Engineering Analysis with Boundary Elements*, 7:178–195.

Grilli, S. T., Voropayev, S., Testik, F. Y., and Fernando, H. J. S. (2003). "Numerical modeling and experiments of wave shoaling over buried cylinders in sandy bottom". In *Proceedings of the 13th Offshore and Polar Engineering Conference*, pages 405–412.

Guerber, E., Benoit, M., Grilli, S. T., and Buvat, C. (2012). "A fully nonlinear implicit model for wave interactions with submerged structures in forced of free motion". *Engineering Analysis with Boundary Elements*, 36:1151–1163.

Guignard, S. and Grilli, S. T. (2001). "Modeling of shoaling and breaking waves in a 2D-NWT by using a spilling breaker model". In *Proceedings of the 11th Offshore and Polar Engineering Conference*, pages 116–123.

Harris, J. C., Dombre, E., Benoit, M., and Grilli, S. T. (2014a). "A comparison of methods in fully nonlinear boundary element numerical wave tank development". In *Proceedings of the 13th Journees de l'Hydrodynamique*.

Harris, J. C., Dombre, E., Benoit, M., and Grilli, S. T. (2014b). "Fast integral equation methods for fully nonlinear water wave modeling". In *Proceedings of the 24th International Offshore and Polar Engineering Conference*, pages 583–590, Busan, Korea.

Harris, J. C., Dombre, E., Mivehchi, A., Benoit, M., Grilli, S. T., and Peyrard, C. (2016). "Progress in fully nonlinear wave modeling for wave-structure interaction". In *Proceedings of the 15th Journée de l'Hydrodynamique*, page 12 pp., Brest, France.

Huseby, M. and Grue, J. (2000). "An experimental investigation of higher-harmonic wave forces on a vertical cylinder". *Journal of Fluid Mechanics*, 414:75–103.

Kim, C. H. (2008). *Nonlinear waves and offshore structures*, volume 27 of *Advanced Series on Ocean Engineering*. World Scientific Pub. Co. Inc. 540 pp.

Longuet-Higgins, M. S. and Cokelet, E. (1976). "The deformation of steep surface waves on water, I. A numerical method of computation". *Proceedings of the Royal Society A*, 350:1–26.

Maestre, J., Cuesta, I., and Pallares, J. (2016). "An unsteady 3D Isogeometrical Boundary Element Analysis applied to nonlinear gravity waves". *Computer Methods in Applied Mechanics and Engineering*, 310:112–133.

Mola, A., Heltai, L., and DeSimone, A. (2013). "A stable and adaptive semi-Lagrangian potential model for unsteady and nonlinear ship-wave interactions". *Engineering Analysis with Boundary Elements*, 37:128–143.

Molin, B. (2002). *Hydrodynamique des structures offshore*. Editions Technip. 440 pp.

Sederberg, T. W., Zheng, J., Bakenov, A., and Nasri, A. (2003). "T-splines and T-NURCCs". *ACM Trans. Graph.*, 22:477–484.

Tanaka, M. (1986). "The stability of solitary waves". *Physics and Fluids*, 29:650–655.

Tanizawa, K. (2000). "The state of the art on numerical wave tank". In *Proceeding of 4th Osaka Colloquium on Seakeeping Performance of Ships*, pages 95–114.